Active site manipulation in MoS_2 cluster electrocatalysts by transition metal doping

Jo J. L. Humphrey[1], Rasmus Kronberg[2], Rongsheng Cai,[3] Kari Laasonen[2], Richard E. Palmer,[3]
Andrew J. Wain*[1]

[1]National Physical Laboratory, Hampton Road, Teddington, TW11 0LW, United Kingdom
[2]Department of Chemistry and Materials Science, Aalto University, P.O. Box 16100, 00076 Aalto, Finland
[3]College of Engineering, Swansea University, Bay Campus, Fabian Way, Swansea, SA1 8EN, United Kingdom

Supporting Information

Cluster Deposition and Characterization

The deposition parameters used for the deposition of the different cluster catalysts are summarized in Table S1. The mass loading deposited on the electrodes was estimated based on the deposition current, deposition time and cluster peak size in the mass distribution.

Table S1. Parameters used for cluster deposition and total mass of clusters deposited on the electrodes.

Sample	**Power on Co target (W)**	**Power on MoS_2 target (W)**	**Pressure in aggregation chamber (mbar)**	**Deposition current (nA)**	**Cluster mass loading on the electrodes (ng)**
MoS_2	/	10	0.50	12.0	11.7
MoS_2-Co(-)	5	10	0.50	10.0	34.8
MoS_2-Co(+)	35	10	0.52	12.2	82.8
Co	35	/	0.43	6.0	78.2

Table S2 presents the elemental percentages of MoS_2 and Co for the hybrid MoS_2-Co(+) and MoS_2-Co(-), as estimated from EDS mapping analysis of STEM HAADF images. Multiple clusters were analysed in each case, and the average Co ratio was calculated from these measurements. Attempts were made to quantify the Co ratio after electrochemical experiments. However, the presence of residual electrolyte salts meant that it was not possible to obtain an EDS signal in this case.

Table S2. Chemical composition of individual MoS_2/Co clusters for MoS_2-Co(+) and MoS_2-Co(-) samples from EDS mapping results.

Sample	Cluster No.	MoS_2 atomic ratio (%)	Co atomic ratio (%)	Co average ratio (%)
MoS_2-Co(+)	1	4.43	95.57	78.04
	2	28.43	71.57	
	3	31.67	68.33	
	4	7.62	92.38	
	5	32.23	67.77	
	6	23.12	76.88	
	7	21.07	78.93	
	8	16.03	83.97	
	9	28.32	71.68	
	10	26.64	73.36	
MoS_2-Co(-)	1	98.86	1.14	2.74
	2	92.58	7.42	
	3	98.83	1.17	
	4	98.76	1.24	

Surface Area Estimation

The total surface area (SA) of the deposited clusters was estimated on the basis of HAADF STEM particle size statistics presented in Figure 2 in the main text. The data used in the calculation is presented in Table S3. The SA and volume per particle were estimated on the assumption of a spherical particle geometry and the particle mass was estimated by assuming a density of 5.1 g cm^{-3} for MoS_2 and 8.9 g cm^{-3} for Co.[1] Since the Co content of MoS_2-Co(-) was determined to be only a few atomic % (see Table S2), the density of this material was assumed to be the same as that of MoS_2. Similarly, the density of MoS_2-Co(+) was assumed to be the same as that of pure Co, on the basis of it being composed of nearly 80% Co. Based on the known mass of clusters deposited for each sample (Table S1), the total number of clusters was estimated, and this was used to estimate the total surface area deposited.

Table S3. Total surface area estimation of deposited clusters

Sample	Cluster diameter (nm)	SA per cluster (cm^2)	Volume per cluster (cm^3)	Mass per cluster (g)	Total mass deposited (g)	Number of clusters deposited	Total SA deposited (cm^2)
MoS_2	5.35	9.0×10^{-13}	8.0×10^{-20}	4.1×10^{-19}	1.17×10^{-8}	2.9×10^{10}	0.026
MoS_2-Co(-)	9.26	2.7×10^{-12}	4.2×10^{-19}	2.1×10^{-18}	3.48×10^{-8}	1.6×10^{10}	0.044
MoS_2-Co(+)	6.99	1.5×10^{-12}	1.8×10^{-19}	1.6×10^{-18}	8.28×10^{-8}	5.2×10^{10}	0.080
Co	5.27	8.7×10^{-13}	7.7×10^{-20}	6.8×10^{-19}	7.82×10^{-8}	1.1×10^{11}	0.100

Whilst the total cluster SA deposited does vary by as much as a factor of four, importantly both of the Co-doped MoS_2 samples exhibit a higher surface area than the pure MoS_2 sample. Therefore, the greater HER performance of pure MoS_2 compared to the Co-doped MoS_2 cannot be rationalized on the grounds of surface area.

Initial Voltammetry and Effect of Scan Rate

Figure S1a depicts the preconditioning cyclic voltammetry performed on pure MoS_2 clusters under static conditions in $HClO_4$ + $NaClO_4$ electrolyte solution (pH 2.8). A small potential shift (20 - 30mV) is observed after the first scan, but after this the voltammetry appears relatively unchanged, indicating sample stability over the timescale of HER performance tests. Figure S1b illustrates LSVs recorded at various scan rates between 1200 mV/s and 2 mV/s for pure MoS_2 clusters. The plot of peak current density against the square root of the scan rate, Figure S1c, shows a linear relationship, thereby confirming that the reaction is under diffusion control, as per the Randles-Ševčík equation.[2] For this analysis, data obtained for scan rates of 10 mV/s and slower were omitted as there was no clearly discernible peak in the LSVs for these scans.

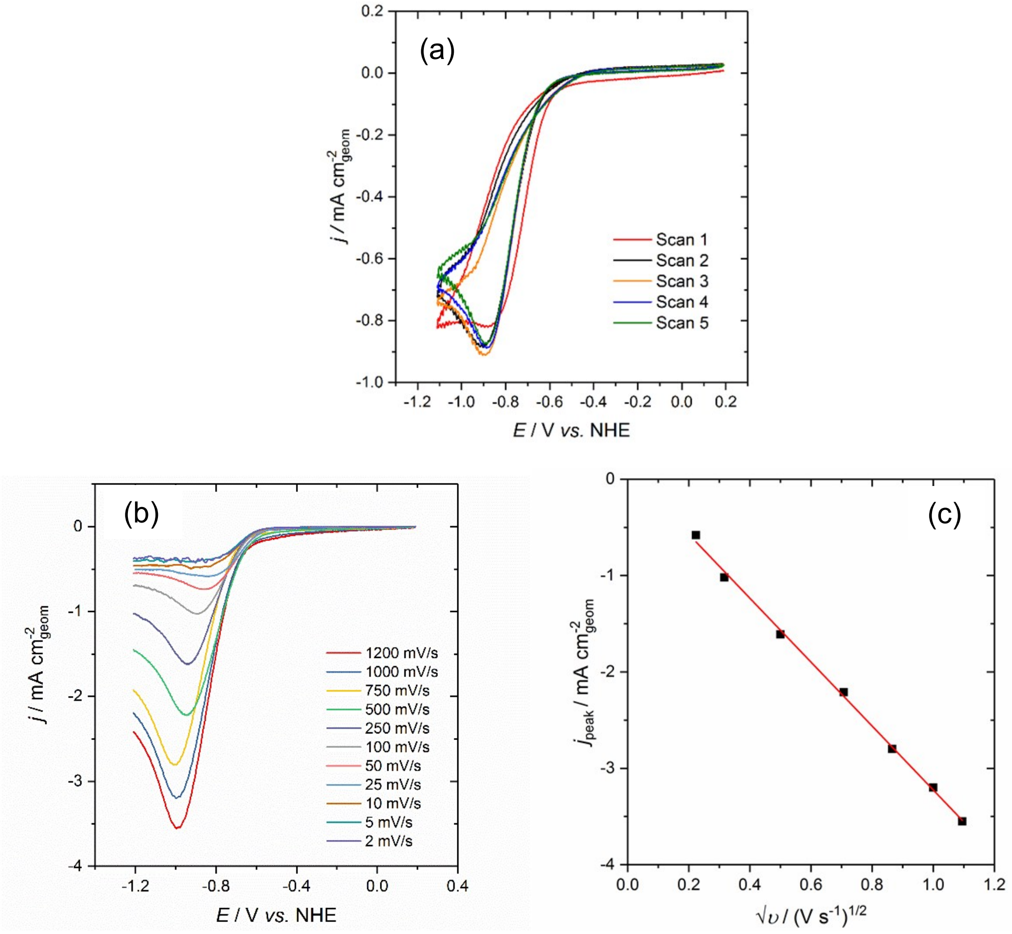

Figure S1. (a) Preconditioning cyclic voltammetry of pure MoS_2 clusters performed at 50 mV/s; (b) LSVs recorded for pure MoS_2 clusters at various scan rates between 1200 mV/s and 2 mV/s; (c) plot of peak current density *vs*. square root of scan rate. Data for scan rates of 10 mV/s and below were omitted as there was no clearly defined peak in the LSVs at these scan rates.

Surface Area Normalization of HER Voltammetry

To verify that the poor HER performance of Co-doped MoS_2 clusters is not related to their differing surface areas, the voltammetric data presented in Figure 4a in the main text was re-normalized to the total cluster SA, as estimated in Table S3. The SA-normalized data is plotted in Figure S2 and for simplicity only the current densities below 0.9 mA cm^{-2} are presented. The data verify that Co doped MoS_2 does not perform as well as pure MoS_2 and Co after SA normalization and suggest that an increase in Co doping level results in an increase in HER overpotential.

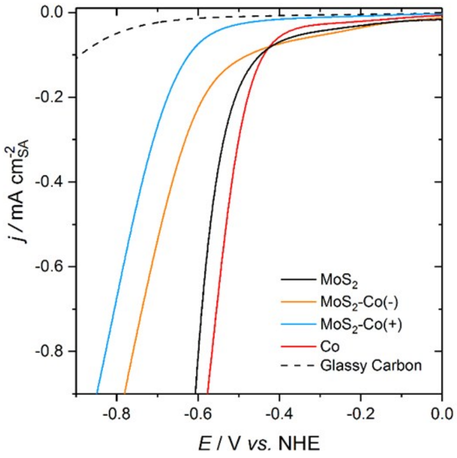

Figure S2. LSVs of the various cluster catalysts, recorded at 25 mV/s in a solution of 0.1 M $NaClO_4$ + 2 mM $HClO_4$ (pH 2.8); the LSV for a bare glassy carbon substrate is also included for comparison. The plotted current densities are normalized to the estimated total surface area of the clusters in each sample.

Electrochemical HER Testing in 0.5 M H_2SO_4

Figure S presents LSVs for the MoS_2, hybrid MoS_2-Co, and Co cluster catalysts recorded in 0.5 M H_2SO_4 (pH ~0) at 5 mV/s under rotation at 1600 rpm. As discussed in the main text, the data validate the experimental trends whereby the pure Co clusters demonstrate the best performance, with an onset potential of approximately -0.15 V, and reaching a current density of -10 mA cm^{-2} at -0.35 V.

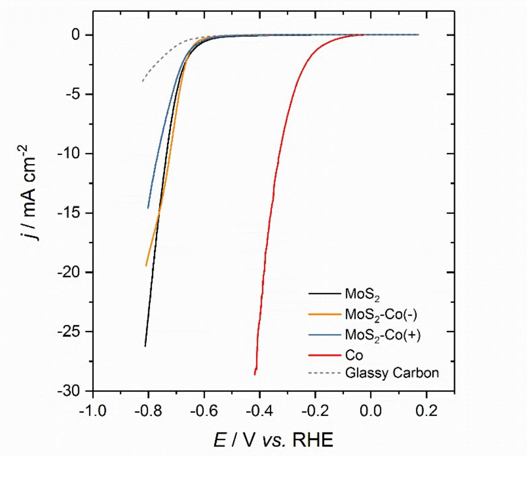

Figure S3. LSVs of the cluster catalyst samples carried out in 0.5 M H_2SO_4 (pH ~0), recorded at 5 mV/s under rotation at 1600 rpm.

Meanwhile, the MoS_2 and MoS_2-Co hybrid clusters all show poor performance compared to pure Co. All three remaining catalysts have onset potentials in the region of -0.6 V and reach the benchmark current density of -10 mA cm^{-2} between approximately -0.75 V and -0.80 V. This confirms the result that Co-doping has no performance-enhancing effect on the catalytic activity of MoS_2 clusters. At higher current densities ($E < -0.7$ V), there is some disparity between these three cluster samples, with MoS_2 outperforming the MoS_2-Co(-) and MoS_2-Co(+) samples and confirming the trend observed in pH 3 electrolyte.

Electronic Structure Calculations

In order to gain insight into the relative stability of the studied systems, we have calculated formation energies of bilayer MoS_2 basal surfaces containing sulfur vacancies and Co/Ni dopants at various separations. Both substitutional and adatom configurations are considered for the dopant atoms. Here, the formation energy ΔE_f of a given structure is defined *via* Eq. S1,

$$\Delta E_f = E_{sys} - E_{ref} - \sum_i n_i \mu_i, \qquad \textbf{Eq. S1}$$

where E_{sys} and E_{ref} are used to denote the total energies of the modified system and the pristine vacancy-free and undoped reference, respectively. The energy difference $E_{sys} - E_{ref}$ is adjusted accordingly by the reference chemical potentials μ_i weighted by the number of atoms n_i added to or removed from the pristine system. For simplicity, since we are mainly interested in studying *relative* stabilities, we neglect vibrational contributions to the chemical potentials. Thus, the chemical potentials are taken to be roughly proportional to the ground state DFT total energies (E_i) of the chosen references, $\mu_i \approx E_i/N_i$, where N_i is the number of atoms in the supercell. Moreover, we note that the evaluation of the energy difference $E_{sys} - E_{ref}$ can be safely considered instead of the *free* energy difference, as most phononic contributions of the target and reference systems will nevertheless cancel due to similarity.[3]

Experimentally, the doped MoS_2 clusters are manufactured using a dual-target magnetron sputtering and gas condensation process (cluster beam deposition). Specifically, MoS_2, Co and Ni sputtering targets have been employed. Therefore, bulk Co(hcp) (288 atoms/supercell) and Ni(fcc) (256 atoms/supercell) were chosen as the reference chemical potentials for the respective elements. The produced MoS_2 clusters are generally reported to be sulfur-deficient,[4, 5] and consequently we treat the Mo and S chemical potentials at the S-poor limit. Following Komsa and Krasheninnikov,[3] we take μ_{Mo} and μ_{MoS_2} to correspond to the bulk Mo(bcc) (250 atoms/supercell) and MoS_2 (72 MoS_2 units/supercell) chemical potentials and fix the sulfur chemical potential *via* Eq. S2,

$$\mu_S = \frac{\mu_{MoS_2} - \mu_{Mo}}{2} \tag{Eq. S2}$$

assuming that MoS_2 is in a thermal equilibrium with Mo and S, which is a reasonable assumption considering the high temperatures (> 1000 K) relevant during cluster formation.[6]

To study the HER activity of the investigated systems, we have probed the hydrogen affinity of various sites on the MoS_2-Co/Ni basal surfaces. The hydrogen adsorption (Volmer reaction) corresponds to a proton-coupled electron transfer (PCET) process,[7] and hence the relevant chemical potential reference for hydrogen is $\mu_H = \mu_{H^+} + \mu_{e^-}$. As a simplification, we apply the computational hydrogen electrode (CHE) scheme introduced by Nørskov *et al.*,[8,9] where an effective equilibrium between solvated protons and electrons and hydrogen in the gas phase at standard conditions is assumed. Hence,

$$\mu_H = \frac{1}{2}\mu_{H_2} + k_B T \ln a_{H^+} - eU_{SHE} = \frac{1}{2}\mu_{H_2} - eU_{RHE} \tag{Eq. S3}$$

and when the applied electrode potential *vs.* the reversible hydrogen electrode (RHE) is further taken to be zero, the free energy of hydrogen adsorption can be estimated simply *via*

$$\Delta G(T,\omega) \approx \Delta F(T,\omega) = \Delta U(T,\omega) - T\Delta S(T,\omega) \tag{Eq. S4}$$

where the internal energy and entropy of the adsorbed system are approximated based on the vibrational contributions. To this end, the partition function of *N* independent harmonic oscillators is invoked,

$$Z = \prod_{i=1}^{3N} \sum_{n=0}^{\infty} e^{-(n+1/2)\beta\hbar\omega_i} \tag{Eq. S5}$$

where ω_i denotes the angular frequency of the *i*th vibrational mode, calculated based on normal mode analyses of adsorbed hydrogen intermediates. Following Reuter and Scheffler,[10] the respective contributions are subsequently obtained as,

$$U(T,\omega) \approx E^{DFT} + E^{vib}(T,\omega) = E^{DFT} - \frac{\partial \ln Z}{\partial \beta} = E^{DFT} + \sum_{i=1}^{3N} \hbar\omega_i \left(\frac{1}{2} + \frac{1}{e^{\beta\hbar\omega_i} - 1} \right) \tag{Eq. S6}$$

and

$$S(T,\omega) \approx S^{vib}(T,\omega) = k\square_B(\ln Z + \beta E^{vib}) = \sum_{i=1}^{3N} k_B \left[\frac{\beta\hbar\omega_i}{e^{\beta\hbar\omega_i} - 1} - \ln\left(1 - e^{-\beta\hbar\omega_i}\right) \right] \tag{Eq. S7}$$

The reference values for E^{vib} and S for the H_2 molecule were taken from thermochemical tables.[11] The results of the atomistic thermodynamics analysis are presented in Table S4.

Table S4. Summary of results from the normal mode analyses of hydrogen adsorbed to various sites on the studied MoS_2 systems at $T = 300$ K.

Adsorption site and system	$\nu_i = \omega_i/2\pi c$ **(cm^{-1})**	E^{vib} **(eV)**	S^{vib} **(10^{-5} eV K^{-1})**
S, MoS_2	2181, 619, 513	0.22	4.60
V_S, MoS_2	1102, 918, 528	0.17	3.45
S, MoS_2-Co(sub)	2566, 697, 655	0.25	2.97
S, MoS_2-Ni(sub)	2585, 677, 659	0.25	3.06
V_S, MoS_2-Co(sub)	1318, 1038, 777	0.20	1.48
V_S, MoS_2-Ni(sub)	1203, 1076, 772	0.19	1.51
Co, MoS_2-Co(ad)	2097, 576, 463	0.21	5.49
Ni, MoS_2-Ni(ad)	2001, 368, 363	0.19	9.61
V_S, MoS_2-Co(ad)	2059, 503, 482	0.20	5.96
V_S, MoS_2-Ni(ad)	1893, 392, 387	0.18	8.78

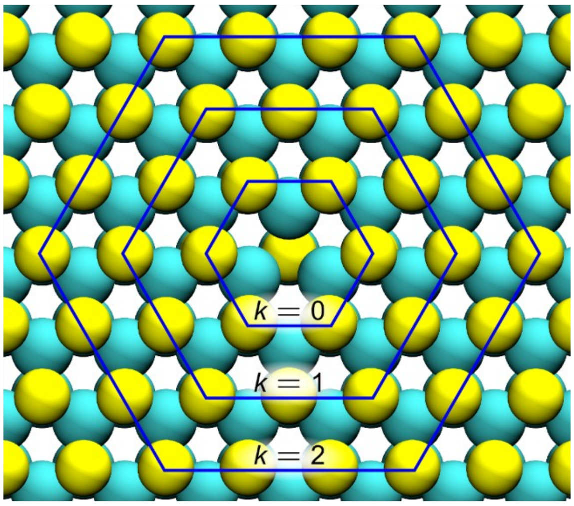

Figure S4. Illustration of the introduced dopant—vacancy separation index k. Doping within the innermost hexagon results a dopant—vacancy separation characterized by $k = 0$, while doping between the inner and the central hexagon, and between the central and the outer hexagon correspond to dopant—vacancy separations $k = 1$ and $k = 2$, respectively.

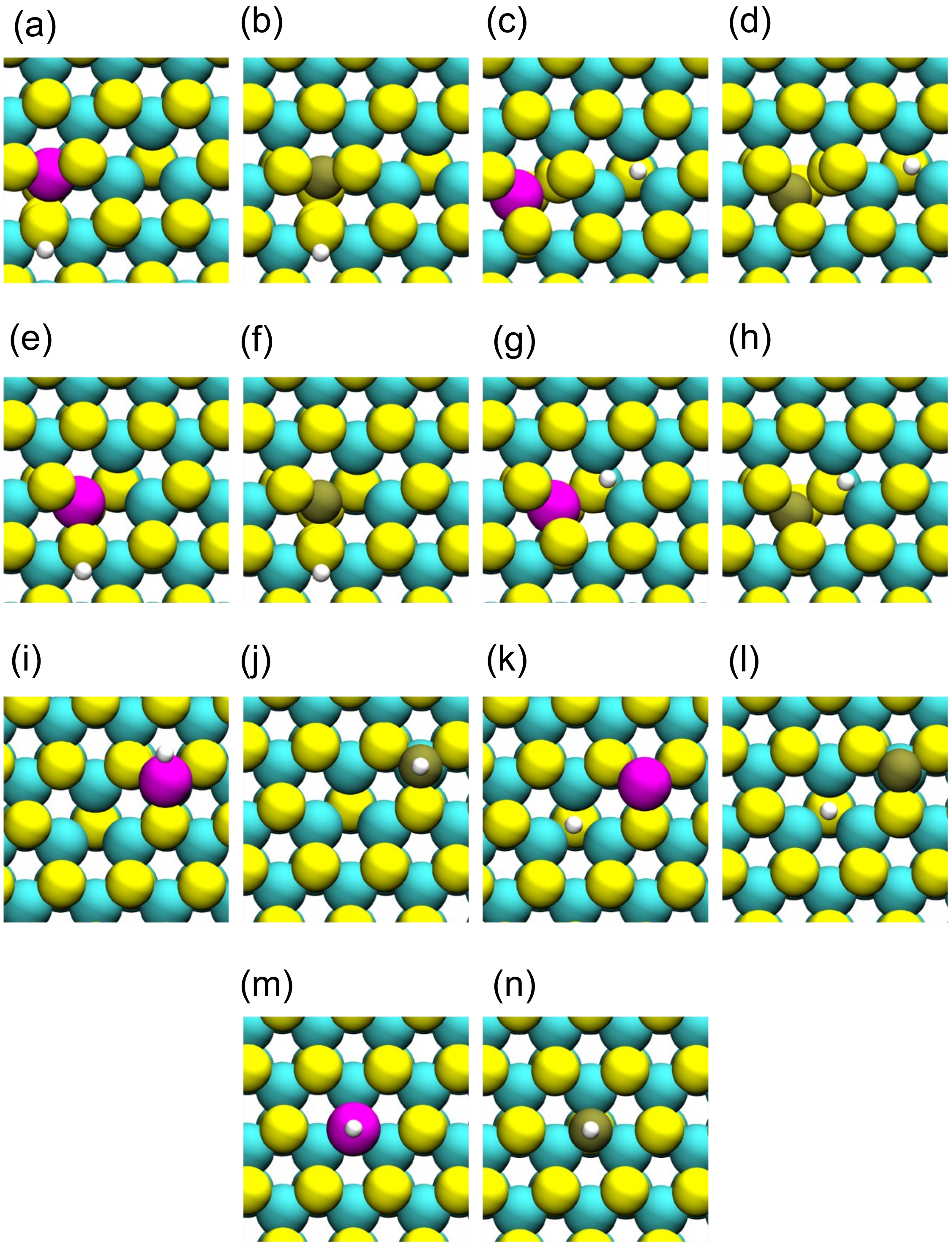

Figure S5. Geometry optimized hydrogen adsorption configurations. (a) S, Co(sub$_1$); (b) S, Ni(sub$_1$); (c) V$_S$, Co(sub$_1$); (d) V$_S$, Ni(sub$_1$); (e) S, Co(sub$_0$); (f) S, Ni(sub$_0$); (g) V$_S$, Co(sub$_0$); (h) V$_S$, Ni(sub$_0$); (i) Co, Co(ad$_1$); (j) Ni, Ni(ad$_1$); (k) V$_S$, Co(ad$_1$); (l) V$_S$, Ni(ad$_1$); (m) Co, Co(ad$_0$); (n) Ni, Ni(ad$_0$). Here, the first symbol denotes the adsorption site, while the second string of characters signifies the dopant—vacancy configuration including the dopant type and distance to vacancy.

References

1. W. M. Haynes, ed., *CRC Handbook of Chemistry and Physics*, CRC Press, Boca Raton, FL, 2011.
2. A. M. Bond, *Broadening Electrochemical Horizons*, Oxford University Press, New York, 2002.
3. H.-P. Komsa and A. V. Krasheninnikov, *Phys. Rev. B*, 2015, **91**, 125304.
4. D. Escalera-López, Y. Niu, J. Yin, K. Cooke, N. V. Rees and R. E. Palmer, *ACS Catal.*, 2016, **6**, 6008-6017.
5. M. J. Cuddy, K. P. Arkill, Z. W. Wang, H.-P. Komsa, A. V. Krasheninnikov and R. E. Palmer, *Nanoscale*, 2014, **6**, 12463-12469.
6. I. M. Goldby, B. von Issendorff, L. Kuipers and R. E. Palmer, *Rev. Sci. Instrum.*, 1997, **68**, 3327-3334.
7. M. T. M. Koper, *Top. Catal.*, 2015, **58**, 1153-1158.
8. J. K. Nørskov, J. Rossmeisl, A. Logadottir, L. Lindqvist, J. R. Kitchin, T. Bligaard and H. Jónsson, *J. Phys. Chem. B*, 2004, **108**, 17886-17892.
9. J. K. Nørskov, T. Bligaard, A. Logadottir, J. R. Kitchin, J. G. Chen, S. Pandelov and U. Stimming, *J. Electrochem. Soc.*, 2005, **152**, J23-J26.
10. K. Reuter and M. Scheffler, *Phys. Rev. B*, 2001, **65**, 035406.
11. P. Linstrom, in *NIST Chemistry WebBook*, 2003.